Anisotropic mesh adaptivity in CFD

Stefano Micheletti Simona Perotto

Dipartimento di Matematica "F. Brioschi"
Politecnico di Milano
via Bonardi 9, 20133 Milano, Italy

1 Why anisotropy?

The straightforward answer to this question could be: *because anisotropy is everywhere!* Actually, when numerically solving a problem in Computational Fluid Dynamics (CFD), or in some other areas, there are many instances where the solution shows *directional features* such as great variations along certain directions with less significant changes along other ones, e.g. boundary and internal layers, singularities or shocks. A typical example is provided by the solution of an advection-diffusion problem, as shown in Fig. 1 [17, 18]. On the

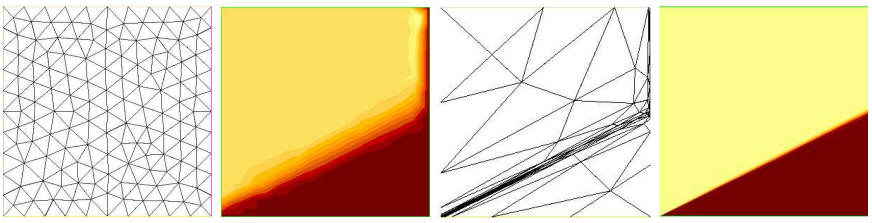

Figure 1: Isotropy (left) versus Anisotropy (right): meshes and contour lines

computational domain $\Omega = (0, 1)^2$, a standard advective-diffusive problem is solved for the scalar u, in the presence of a convective field $\mathbf{a} = (2, 1)^T$ and with a diffusivity $\mu = 10^{-4}$, completed with Dirichlet boundary conditions, i.e. $u = 1$ on the left and top sides and $u = 0$ on the remaining ones. The solution u exhibits an internal and a boundary layer of thickness $\mathcal{O}(10^{-2})$ and $\mathcal{O}(10^{-4})$, respectively. As Fig. 1 shows, the isotropic mesh consists of more elements than the corresponding anisotropic one (312 versus 64 triangles). In the latter case a correct orientation and deformation of the mesh elements (longest edges parallel to the boundary layers) yields a great reduction of the number of triangles. Moreover, in the anisotropic case the layers are captured more sharply.

This simple but remarkable example highlights the "leitmotiv" of an anisotropic analysis: for a fixed solution accuracy, reduce the number of degrees of freedom involved in the approximation of the problem at hand by better orienting the

mesh elements according to some suitable features of the solution, or vice versa, given a constraint on the number of elements, find the mesh maximizing the accuracy of the numerical solution.

Going back to the utility of anisotropy, we observe that things may not be so straightforward, of course. While anisotropy is proved to be superior in terms of effectiveness for the most accurate computations in many cases, yet, there are some instances where a structured Adaptive Mesh Refinement (AMR) procedure turns out to be more simple to carry out, especially in view of an implementation in a parallel environment. Moreover, in the unstructured case, the main drawback of the anisotropic approach compared to the isotropic one, is the more complex analysis required to fully describe the element dimensions and orientation. Though, this heavier burden is the strength of the method. For other approaches in the anisotropic context, see e.g. [1, 7, 8, 15, 19].

The outline of the article is the following. In Sect. 2 we introduce the anisotropic framework by recalling some anisotropic interpolation error estimates, representing the main tool used in the a posteriori error analysis addressed in Sect. 3. This analysis is discussed in the case of a general differential operator, moving from the adjoint theory for goal-oriented error control, and it is then detailed for the advection-diffusion-reaction and the Stokes problems. Finally, in Sect. 4 the effectiveness of the anisotropic philosophy is assessed on some numerical test cases.

2 The anisotropic setting for FEM

Let $\Omega \subset \mathbb{R}^2$ be a polygonal domain and, for any $0 < h \leq 1$, let $\{\mathcal{T}_h\}_h$ be a family of conforming triangulations of $\overline{\Omega}$ into triangles K of diameter $h_K \leq h$. Following the idea proposed in [10], in order to derive the additional information for the geometrical description of the mesh triangles, we move from the standard affine transformation $T_K : \widehat{K} \to K$, with $K = M_K(\widehat{K}) + \mathbf{b}_K$, $M_K \in \mathbb{R}^{2\times 2}$ and $\mathbf{b}_K \in \mathbb{R}^2$, from the reference triangle $\widehat{K}$ into K, where $\widehat{K}$ can be, e.g., the right triangle $(0,0),(1,0),(0,1)$ or the equilateral one $(-1/2,0),(1/2,0),(0,\sqrt{3}/2)$ (see Fig. 2). Let $M_K = B_K\, Z_K$ be the polar decomposition of the invertible

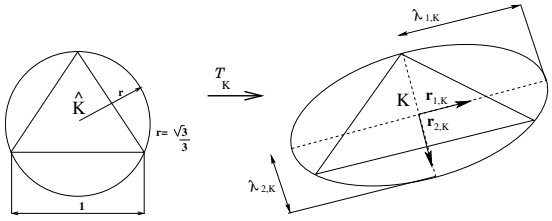

Figure 2: The map T_K

matrix M_K, with B_K and Z_K a symmetric positive definite and an orthogonal matrix, respectively. Then we factorize the matrix B_K in terms of its eigenvalues

$\lambda_{i,K}$ (with $\lambda_{1,K} \geq \lambda_{2,K}$) and eigenvectors $\mathbf{r}_{i,K}$, for $i = 1, 2$, as $B_K = R_K^T \Lambda_K R_K$, where $\Lambda_K = \mathrm{diag}(\lambda_{1,K}, \lambda_{2,K})$ and $R_K = [\mathbf{r}_{1,K}, \mathbf{r}_{2,K}]^T$. As Fig. 2 shows, the eigenvectors $\mathbf{r}_{i,K}$ provide the directions of the semi-axes of the ellipse circumscribed to the element K, while the eigenvalues $\lambda_{i,K}$ measure the length of such semi-axes. Thus, the shape and orientation of each triangle K is completely described by the quantities $\mathbf{r}_{i,K}$ and $\lambda_{i,K}$. The deformation of K with respect to $\widehat{K}$ can be measured by the so-called *stretching factor* $s_K = \lambda_{1,K}/\lambda_{2,K} (\geq 1)$, being $s_{\widehat{K}} = 1$.

2.1 Functional framework

Throughout, we use a standard notation to denote the Sobolev spaces of functions with Lebesgue-measurable derivatives, and their norms [16]. In more detail, let $W^{k,p}(\Omega)$ be the Sobolev space of functions for which th p-th power of the absolute value of their distributional derivatives of order up to $k \geq 0$ is Lebesgue-measurable, with $1 \leq p < \infty$. For $p = 2$ we let $H^k(\Omega) = W^{k,2}(\Omega)$. In particular, $L^2(\Omega)$ is the space of square-integrable functions with norm $\|\cdot\|_{L^2(\Omega)}$ and scalar product $(\cdot,\cdot)$, while for the space $H^k(\Omega)$ we denote by $\|\cdot\|_{H^k(\Omega)}$ and $|\cdot|_{H^k(\Omega)}$ the corresponding norm and seminorm, respectively. When the norms or seminorms are referred to some subspace S of Ω, they are written as $\|\cdot\|_{L^2(S)}$, $\|\cdot\|_{H^k(S)}$ and $|\cdot|_{H^k(S)}$, while the scalar product is denoted by $(\cdot,\cdot)_S$. We also recall that $L^\infty(\Omega)$ is the space of bounded functions a.e., while $W^{1,\infty}(\Omega) \subset L^\infty(\Omega)$ is such that also the first derivatives are bounded a.e. Finally, $C^0(\overline{\Omega})$ denotes the space of continuous functions on $\overline{\Omega}$.

2.2 Anisotropic interpolation error estimates

The starting point for the a posteriori analysis in Sect. 3 has been the derivation of suitable anisotropic interpolation error estimates [10, 12, 17].
We have proved estimates for both the Lagrange and the Clément-like interpolants [5, 6] to take into account different regularity of the function to be interpolated. Denoting by W_h the finite element space of continuous affine functions, let $\Pi_h : C^0(\overline{\Omega}) \to W_h$ and $I_h : L^2(\Omega) \to W_h$ be the Lagrange and Clément linear interpolants, respectively and let their restrictions to each element $K \in \mathcal{T}_h$ be Π_K and I_K. Then we have:

Proposition 2.1 *Let $v \in H^2(K)$, for any $K \in \mathcal{T}_h$. Then there exist two constants $C_1 = C_1(\widehat{K})$ and $C_2 = C_2(\widehat{K})$ such that*

$$\|v - \Pi_K(v)\|_{L^2(K)} \leq C_1 \left[\sum_{i,j=1}^{2} \lambda_{i,K}^2 \lambda_{j,K}^2 L_K^{i,j}(v) \right]^{1/2}, \tag{1}$$

$$|v - \Pi_K(v)|_{H^1(K)} \leq C_2 \, \lambda_{2,K}^{-1} \left[\sum_{i,j=1}^{2} \lambda_{i,K}^2 \lambda_{j,K}^2 L_K^{i,j}(v) \right]^{1/2}, \tag{2}$$

where

$$L_K^{i,j}(v) = \int_K \left(\mathbf{r}_{i,K}^T\, H_K(v)\, \mathbf{r}_{j,K}\right)^2 \, d\mathbf{x}, \quad \textit{with} \;\; i,\, j = 1,\, 2, \tag{3}$$

and $H_K(v)$ is the Hessian matrix associated with v.

Proposition 2.2 *Let $v \in H^1(\Omega)$. Then there exist two constants $C_3 = C_3(M, \widehat{C})$ and $C_4 = C_4(M, \widehat{C})$ such that, for any $K \in \mathcal{T}_h$,*

$$\|v - I_K(v)\|_{L^2(K)} \leq C_3 \left[\sum_{i=1}^{2} \lambda_{i,K}^2 \left(\mathbf{r}_{i,K}^T G_K(v) \mathbf{r}_{i,K}\right)\right]^{1/2}, \tag{4}$$

$$|v - I_K(v)|_{H^1(K)} \leq C_4\, \lambda_{2,K}^{-1} \left[\sum_{i=1}^{2} \lambda_{i,K}^2 \left(\mathbf{r}_{i,K}^T G_K(v) \mathbf{r}_{i,K}\right)\right]^{1/2}, \tag{5}$$

where $G_K(v) \in \mathbb{R}^{2\times 2}$ is the symmetric positive semi-definite matrix with entries $(G_K(v))_{i,\,j} = \int_{\Delta_K} \partial v/\partial x_i \; \partial v/\partial x_j \, d\mathbf{x}$ with $\mathbf{x} = (x_1,\, x_2)^T \in K$, Δ_K is the patch of all the elements sharing a vertex with K, and $M \in \mathbb{N}$ and $\widehat{C} > 0$ are the constants defined through the relations

$$\mathrm{card}(\Delta_K) \leq M \quad \textit{and} \quad \mathrm{diam}(\Delta_{\widehat{K}}) \leq \widehat{C}\,, \tag{6}$$

with $\Delta_{\widehat{K}} = T_K^{-1}(\Delta_K)$.

Remark 2.1 *Requirements (6) demand the cardinality of any patch Δ_K as well as the diameter of the reference patch $\Delta_{\widehat{K}}$ to be uniformly bounded independently of the geometry of the mesh. In particular, the latter inequality rules out some too distorted reference patches (see Fig. 1.1 in [17]).*

A comparison of the inequalities in Proposition 2.1 and 2.2 with the corresponding isotropic results shows that the anisotropic estimates are more complex. For instance, let us consider the isotropic estimate corresponding to (1), given by

$$\|v - \Pi_K(v)\|_{L^2(K)} \leq C_1^*\, h_K^2\, |v|_{H^2(K)}\,, \tag{7}$$

with $C_1^* = C_1^*(\widehat{K})$. From a dimensional viewpoint, we have both in (1) and in (7) the square of the spacing parameters (i.e. h_K in the isotropic case, $\lambda_{1,K}$, $\lambda_{2,K}$ in the anisotropic one). On the other hand, the H^2-seminorm of v in (7) is replaced by a suitable sum of the $L_K^{i,j}(v)$ quantities in (1). We claim that the information provided by the seminorm $|v|_{H^2(K)}$ has been split along the directions $\mathbf{r}_{1,K}$ and $\mathbf{r}_{2,K}$ via the quantities $L_K^{i,j}(v)$ representing squared L^2-norms of directional second-order derivatives of v. As anticipated in Sect. 1, we are replacing the "lumped" isotropic results with more "distributed" ones. The pay-off of such a framework is that we are able to finely tune the adapted meshes in terms of shape and orientation of the elements.
Finally, in view of the a posteriori analysis of Sect. 3, we have also derived anisotropic estimates for the L^2-norm of the interpolation error on the edges e of the triangulation $\mathcal{T}_h$ (see [12] for the details).

3 Anisotropic a posteriori error analysis

Moving from the a posteriori dual-based approach developed in [3], we aim to control suitable linear continuous functionals $J(\cdot)$ of the discretization error e_h associated with the considered finite element approximation. In CFD, examples of $J(\cdot)$ are the lift and drag around bodies in external flows or mean and local values, while in structural mechanics the torsion moment, the stress value or the surface tension are typical goal-quantities. The leading idea of our a posteriori analysis has been to combine the advantages deriving from an error functional control with the richness of information provided by an anisotropic framework.

Let us sketch the procedure used to derive the anisotropic a posteriori error estimator for a general differential problem

$$L(u) = f \quad \text{in } \Omega\,. \tag{8}$$

In the subsections below we particularize such a procedure to standard model problems in CFD. We refer to [11, 12, 13] for a detailed description of such an approach.
First, let us introduce the weak form associated with (8): find $u \in V$ such that

$$a(u, v) = F(v) \quad \text{for any} \quad v \in V, \tag{9}$$

where V is a suitable functional space accounting for the boundary conditions completing the problem at hand, and $a(\cdot, \cdot)$ and $F(\cdot)$ are the bilinear and linear forms corresponding to the differential operator L and the source term f in (8), respectively. The discrete form associated with (9) is obtained by projection onto the space $V_h \subset V$ of continuous piecewise linear finite elements which yields: find $u_h \in V_h$ such that

$$a(u_h, v_h) = F(v_h) \quad \text{for any} \quad v_h \in V_h. \tag{10}$$

As shown in Sects. 3.1 and 3.2, the forms $a(\cdot, \cdot)$ and $F(\cdot)$ have to be suitably stabilized in the case of strong advective/reactive terms, or of the Stokes problems in order to guarantee the absence of spurious oscillations or the well-posedness of the problem, respectively.
By suitably combining the weak form, with $v = v_h$, with the discrete one, we get the well-known Galerkin orthogonality property

$$a(e_h,\, v_h) = 0 \quad \text{for any} \quad v_h \in V_h, \tag{11}$$

stating the orthogonality of the discretization error $e_h = u - u_h$ with respect to the discrete space V_h.
Let us introduce now the dual problem associated with (9): find $z \in V$ such that

$$a^*(z,\, \varphi) = J(\varphi) \quad \text{for any} \quad \varphi \in V, \tag{12}$$

where J is a linear continuous functional to be suitably chosen according to the physical quantity to control and $a^*(\cdot,\cdot)$ is the adjoint form to $a(\cdot,\cdot)$, defined by the relation $a^*(z,\,\varphi) = a(\varphi, z)$, for any $\varphi \in V$.

We are now in a position to estimate the discretization error associated with the goal quantity, i.e. $J(e_h)$. With this aim, let us first choose in (12) $\varphi = e_h$. Then by exploiting the property of the adjoint form $a^*(\cdot,\cdot)$ and the Galerkin orthogonality property (11) with $v_h = z_h$, we get

$$J(e_h) = a^*(z,\, e_h) = a(e_h,\, z) = a(e_h,\, z - z_h) = F(z - z_h) - a(u_h,\, z - z_h), \tag{13}$$

where the last equality is due to the weak form (9) with $v = z - z_h$. So far no explicit choice has been made for z_h. Usually, z_h is identified with a suitable interpolant of the dual solution z, according to the regularity of the latter. An integration by parts of the right-hand side of (13) together with a suitable use of anisotropic interpolation error estimates such as those cited in Sect. 2.2, lead to an a posteriori error estimate of the general form

$$|J(e_h)| \le C \sum_{K \in \mathcal{T}_h} \rho_K(u_h)\, \omega_K(z), \tag{14}$$

where $\rho_K(u_h) = f - L(u_h)$ is the residual associated with the the primal problem (8) and $\omega_K(z)$, which gathers the anisotropic information, depends on the dual solution and weights the residual term. Notice that $\rho_K(u_h)$ measures the error related to the approximation u_h, while the term $\omega_K(z)$ takes into account the propagation of such an error driven by the functional $J(\cdot)$ to control. The terms $\rho_K(u_h)$ and $\omega_K(z)$ in (14) depend on the particular differential problem (8). In the subsections below we explicitly provide two examples of the estimator (14) by considering some standard problems.

3.1 The advection-diffusion-reaction problem

We address the standard scalar advection-diffusion-reaction problem with mixed boundary conditions

$$\begin{cases} L(u) = -\mu\,\Delta u + \mathbf{a}\cdot\nabla u + \alpha\, u = f & \text{in } \Omega\,, \\ u = 0 & \text{on } \Gamma_D\,, \\ \mu\,\dfrac{\partial u}{\partial n} = g & \text{on } \Gamma_N \end{cases} \tag{15}$$

where Γ_D and Γ_N are suitable measurable nonoverlapping partitions of the boundary $\partial\Omega$ of Ω with $\Gamma_D \neq \emptyset$ and such that $\partial\Omega = \overline{\Gamma}_D \cup \overline{\Gamma}_N$; the source $f \in L^2(\Omega)$, the diffusivity $\mu \in \mathbb{R}^+$, the advective field $\mathbf{a} \in (W^{1,\infty}(\Omega))^2$, with $\nabla\cdot\mathbf{a} = 0$, the reaction coefficient $\alpha \in L^\infty(\Omega)$ with $\alpha \ge 0$ a.e. in Ω, and $g \in L^2(\Gamma_N)$ are given data, while $\partial u/\partial n = \nabla u \cdot \mathbf{n}$ is the normal derivative of u, $\mathbf{n}$

being the unit outward normal to $\partial\Omega$.
As we are interested in advection-reaction dominated problems, we have to discretize (15) by means of a suitable stabilized scheme. The discrete form (10) is thus replaced by the stabilized one

$$a_\tau(u_h, v_h) = F_\tau(v_h) \quad \text{for any} \quad v_h \in V_h. \tag{16}$$

For instance, by choosing a streamline-diffusion scheme [9], the stabilized forms $a_\tau : V \times V \to \mathbb{R}$ and $F_\tau : V \to \mathbb{R}$ for smooth enough functions u and v, are defined as

$$\begin{aligned} a_\tau(u,v) &= \int_\Omega \mu \nabla u \cdot \nabla v \, d\mathbf{x} + \int_\Omega (\mathbf{a} \cdot \nabla u + \alpha\, u) v \, d\mathbf{x} \\ &+ \sum_{K \in \mathcal{T}_h} \int_K \tau_K \left(-\mu \Delta u + \mathbf{a} \cdot \nabla u + \alpha\, u\right) (\mathbf{a} \cdot \nabla v) \, d\mathbf{x}\,, \\ F_\tau(v) &= \int_\Omega f\, v \, d\mathbf{x} + \int_{\Gamma_N} g\, v \, ds + \sum_{K \in \mathcal{T}_h} \int_K \tau_K \, f (\mathbf{a} \cdot \nabla v) \, d\mathbf{x}\,, \end{aligned}$$

where the coefficients τ_K are elementwise stabilizing parameters for which several proposals can be found in the literature (see, e.g., [2, 3, 4, 17]).
Following the procedure described above, we can derive an anisotropic a posteriori error estimator for (15) which can be cast in the form (14) [13]. Let us define the element interior and boundary residuals given by $r_K = (f + \mu \Delta u_h - \mathbf{a} \cdot \nabla u_h - \alpha\, u_h)|_K$ and

$$j_e = \begin{cases} 0 & \text{if } \; e \in \Gamma_D\,, \\ -2 \left(\mu \dfrac{\partial u_h}{\partial n_K} - g \right) & \text{if } \; e \in \Gamma_N\,, \\ -\mu \left[\dfrac{\partial u_h}{\partial n_K} \right]_e & \text{if } \; e \in \mathcal{E}_h^{\text{int}}\,, \end{cases} \tag{17}$$

respectively. Here $\partial u_h / \partial n_K = \nabla u_h \cdot \mathbf{n}_K$ is the normal derivative of u_h, $\mathbf{n}_K$ is the unit outward normal to ∂K, $\mathcal{E}_h^{\text{int}}$ denotes the set of the internal edges of the skeleton $\mathcal{E}_h$ of the triangulation $\mathcal{T}_h$, and $[\partial u_h / \partial n_K]_e$ stands for the jump of the normal derivative of u_h over the edge $e \subset \partial K$. Then the residual $\rho_K(u_h)$ is given by

$$\rho_K(u_h) = \|r_K(u_h)\|_{L^2(K)} \left(1 + \frac{\tau_K}{\lambda_{2,K}} \|\mathbf{a}\|_{L^\infty(K)} \right) + \frac{1}{2 \lambda_{2,K}^{1/2}} \|j_e\|_{L^2(\partial K)}\,. \tag{18}$$

Concerning the weight $\omega_K(z)$, by assuming an H^1-regularity for the dual solution z, we identify z_h in (13) with the Clément interpolant of z, thus obtaining

$$\omega_K(z) = \left[\sum_{i=1}^{2} \lambda_{i,K}^2 \, \left(\mathbf{r}_{i,K}^T \, G_K(z) \mathbf{r}_{i,K} \right) \right]^{1/2}. \tag{19}$$

Notice that all the anisotropic information $\lambda_{i,K}$ and $\mathbf{r}_{i,K}$ is contained in (19). The a posteriori analysis above has been applied to a more realistic problem in haemodynamics [11]. Moreover, the analysis above covers also the diffusion-reaction problem by letting $\mathbf{a} = \mathbf{0}$ in (15).

3.2 The Stokes problem

Let us consider the standard Stokes problem: seek the velocity $\mathbf{u}$ and the pressure p of an incompressible fluid, subject to mixed boundary conditions:

$$\begin{cases} -\mu\Delta\mathbf{u} + \nabla p = \mathbf{f} & \text{in } \Omega\,, \\ \nabla\cdot\mathbf{u} = 0 & \text{in } \Omega\,, \\ \mu\,(\nabla\mathbf{u})\,\vec{n} - p\,\vec{n} = \mathbf{g} & \text{on } \Gamma_N\,, \\ \mathbf{u} = \mathbf{0} & \text{on } \Gamma_D\,, \end{cases} \tag{20}$$

where Γ_D, Γ_N and $\vec{n}$ are defined as in Sect. 3.1; the source term $\mathbf{f} \in [L^2(\Omega)]^2$, the viscosity $\mu \in \mathbb{R}^+$, $\mathbf{g} \in [L^2(\Gamma_N)]^2$ are given data. Notice that the differential operator $L(u)$ in (8) is replaced by the operator $L(\mathbf{u}, p)$ given by the left-hand sides of $(20)_1$-$(20)_2$. Moreover, the weak space V in (9) is replaced by the tensor product space $W \times Q$.
In order to guarantee the inf-sup condition, the discretization of the Stokes problem requires a stabilized method. By using, for instance, the Galerkin Least Squares method, the stabilized discrete form of (20) becomes: find $(\mathbf{u}_h, p_h)$ in $W_h \times Q_h$, with $W_h \subset W$ and $Q_h \subset Q$ formed by continuous piecewise linear finite elements, such that

$$a_\tau((\mathbf{u}_h, p_h), (\mathbf{v}_h, q_h)) = F_\tau(\mathbf{v}_h, q_h) \quad \text{for any} \quad (\mathbf{v}_h, q_h) \in W_h \times Q_h, \tag{21}$$

where the stabilized forms $a_\tau : [W \times Q]^2 \to \mathbb{R}$ and $F_\tau : W \times Q \to \mathbb{R}$ are given by

$$\begin{aligned} a_\tau((\mathbf{u}, p), (\mathbf{v}, q)) = & \int_\Omega \mu\nabla\mathbf{u} : \nabla\mathbf{v}\, d\mathbf{x} - \int_\Omega p\nabla\cdot\mathbf{v}\, d\mathbf{x} - \int_\Omega q\,\nabla\cdot\mathbf{u}\, d\mathbf{x} \\ & - \sum_{K\in\mathcal{T}_h} \tau_K \int_K \nabla p\cdot\nabla q\, d\mathbf{x} \\ F_\tau(\mathbf{v}, q) = & \int_\Omega \mathbf{f}\cdot\mathbf{v}\, d\mathbf{x} + \int_{\Gamma_N} \mathbf{g}\cdot\mathbf{v}\, ds - \sum_{K\in\mathcal{T}_h} \tau_K \int_K \mathbf{f}\cdot\nabla q\, d\mathbf{x}. \end{aligned} \tag{22}$$

As we have two unknowns, we can control two continuous linear functionals, the first one $J_1(\cdot)$ associated with the discretization error $\vec{e}_u = \mathbf{u} - \mathbf{u}_h$ of the velocity and the second one $J_2(\cdot)$ related to the discretization error $e_p = p - p_h$ of the pressure. Likewise, we can define both the element interior and boundary residuals associated with the momentum equation $(20)_1$, $\boldsymbol{r}_K^1(\mathbf{u}_h, p_h) = (\mathbf{f} +$

$\mu\Delta\mathbf{u}_h - \nabla p_h)|_K$ and

$$\boldsymbol{\mathcal{J}}_e = \begin{cases} \mathbf{0} & \text{if } e \in \Gamma_D\,, \\ 2\,(\mathbf{g} - (\mu(\nabla\mathbf{u}_h\,\vec{n}_K) - p_h\,\vec{n}_K)) & \text{if } e \in \Gamma_N\,, \\ -\,[(\mu(\nabla\mathbf{u}_h\,\vec{n}_K) - p_h\,\vec{n}_K)]_e & \text{if } e \in \mathcal{E}_h^{\text{int}}\,, \end{cases} \tag{23}$$

respectively, and the interior residual $r_K^2(\mathbf{u}_h) = (\nabla\cdot\mathbf{u}_h)|_K$ related to the continuity equation $(20)_2$. Estimate (14) is thus replaced by the new one

$$|J_1(\vec{e}_u) + J_2(e_p)| \leq C \sum_{K\in\mathcal{T}_h} (\rho_K^1(\mathbf{u}_h, p_h)\,\omega_K^1(\vec{w}) + \rho_K^2(\mathbf{u}_h, p_h)\,\omega_K^2(r))\,, \tag{24}$$

with $C = C(M, \widehat{C}, \widehat{K})$ and $(\vec{w}, r)$ the dual velocity-pressure pair, while

$$\begin{aligned} \rho_K^1(\mathbf{u}_h, p_h) &= ||\boldsymbol{r}_K^1(\mathbf{u}_h, p_h)||_{L^2(K)} + \frac{1}{2}||\boldsymbol{\mathcal{J}}_e||_{L^2(\partial K)}\left(\frac{\lambda_{1,K}^2 + \lambda_{2,K}^2}{\lambda_{2,K}^3}\right)^{1/2}, \\ \rho_K^2(\mathbf{u}_h, p_h) &= ||r_K^2(\mathbf{u}_h)||_{L^2(K)} + \frac{\tau_K}{\lambda_{2,K}}\,||\boldsymbol{r}_K^1(\mathbf{u}_h, p_h)||_{L^2(K)}, \\ \omega_K^1(\vec{w}) &= \Big[\sum_{i,j=1}^{2} \lambda_{i,K}^2\lambda_{j,K}^2 L_K^{i,j}(\vec{w})\Big]^{1/2}, \omega_K^2(r) = \Big[\sum_{i=1}^{2}\lambda_{i,K}^2\left(\mathbf{r}_{i,K}^T G_K(r)\mathbf{r}_{i,K}\right)\Big]^{1/2}, \end{aligned} \tag{25}$$

where $L_K^{i,j}(\vec{w})$ is the straightforward extension to vector-valued functions of the term (3). We point out that (24) consists of contributions associated with the error propagation due to both the dual velocity and the dual pressure.

4 Numerical results

A typical numerical solution process of a given problem consists of an adaptive iterative procedure based on a metric-based approach. Starting from the a posteriori error estimate, a second-order tensor field, embedding the information about the mesh spacing and stretching, is defined on the actual mesh and employed for the generation of the new mesh, as described in [13]. The software BAMG [14] has been used for this purpose.
In this section we address the numerical solution of some test cases. In more detail, we consider the advection-diffusion-reaction problem (15) and we show the effectiveness of the adaptive algorithm for the construction of an "optimal " mesh, e.g., the mesh for which we have maximum accuracy for a given number of degrees of freedom.
The "glass" test case
Let us define $r = \sqrt{(x_1 - 1/2)^2 + (x_2 - 1/2)^2}$ while choosing in (15), $\Omega = (0,1)^2$, $\mu = 10^{-4}$, $f = 1$ for $1/5 < r < 1/4$ and zero elsewhere, $\mathbf{a} = (x_2 - 1/2, -(x_1 - 1/2))^T$, $\alpha = 100$ for $r < 1/5$ and zero elsewhere, and $\Gamma_N = \emptyset$. The

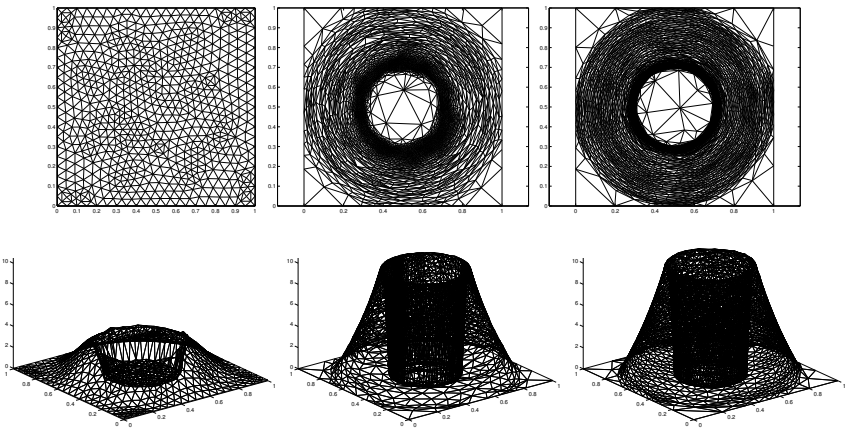

Figure 3: Sequence of meshes (top) and corresponding solutions (bottom)

Table 1: Degrees of freedom: the "glass" (left) and "channel" (right) test cases

# elements	# nodes
1312	697
4203	2123
5838	2939

# elements	# nodes
1016	561
3763	1950
3991	2083

solution u exhibits a strong internal circular layer in the region $1/5 < r < 1/4$ and a large gradient in the radial direction in the region $1/4 < r < 1$. With reference to Fig. 3, the adaptive process starts from a uniform mesh (top-left) and is stopped after two iterations, yielding the meshes at the top-center and top-right. The numerical solutions on the initial mesh, and on the other two meshes are displayed in the bottom line. The functional $J(\cdot)$ has been chosen as $J(v) = a_0(v, u)$ for any $v \in V$, where the subscript 0 refers to the nonstabilized bilinear form derived from (16). This choice allows us to control the energy norm of the discretization error, as $J(u - u_h) = a_0(u - u_h, u) = a_0(u - u_h, u - u_h)$, thanks to the Galerkin orthogonality property. All the main directional features characterizing the solution u are well captured by the anisotropic error estimator as the mesh elements are stretched along the direction of the layers. Table 1 (left) collects the information about the number of elements and of nodes for the three meshes.

The "channel" test case

Let Ω in (15) be the U-shaped domain given by the square $(-1, 1)^2$ from which the rectangle $(-1, 0) \times (-0.4, 0.4)$ has been cut, and $\mu = 10^{-4}$, $f = 0$, $\mathbf{a} = (x_2, -x_1)^T$, $\alpha = 0$, and $\Gamma_N = \emptyset$. The nonhomogeneous Dirichlet datum takes the value 1 on the sides $(\{x_1 = -1\} \cap \{0.4 \leq x_2 \leq 1\}) \cup (\{x_2 = 0.4\} \cap \{-1 \leq x_1 \leq -0.5\})$. The solution shows two circular-shaped internal layers, a boundary layer near the top-left corner at $x_2 = 1$, and an outflow boundary layer at

$x_2 = -0.4$. With reference to Fig. 4, the adaptive process starts from a uniform mesh (top-left) and is iterated two more times, with corresponding grids shown at top-center and top-right. The numerical solutions on the initial mesh and on the two adapted meshes are displayed in the bottom line. The functional $J(\cdot)$ has been chosen as in the previous example. Notice how all the layers are well represented on the last grid, though some oscillation is still polluting the numerical solution. Table 1 (right) summarizes the information about the number of elements and of nodes for the sequence of meshes.

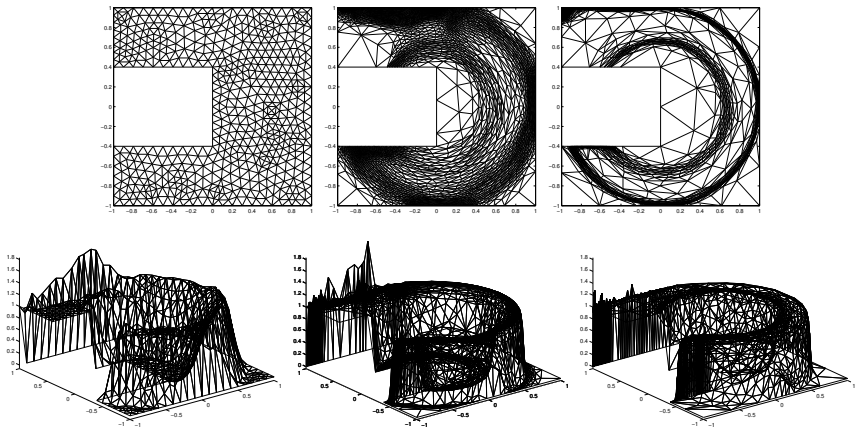

Figure 4: Sequence of meshes (top) and corresponding solutions (bottom)

5 Acknowledgments

This work has been supported by the project MIUR 2001 "Numerical Methods in Fluid Dynamics and Electromagnetism". We thank Prof. Luca Formaggia for useful comments and suggestions over our enduring collaboration.

References

[1] Apel, T.: Anisotropic Finite Elements: Local Estimates and Applications. Book Series: Advances in Numerical Mathematics, Teubner, Stuttgart (1999)

[2] Apel, L., Lube, G.: Anisotropic mesh refinement in stabilized Galerkin methods. Numer. Math., **74**, 261–282 (1996)

[3] Becker, R., Rannacher, R.: An optimal control approach to a posteriori error estimation in finite element methods. Acta Numerica, **10**, 1–102 (2001)

[4] Brezzi, F., Russo, A.: Choosing bubbles for advection-diffusion problems. Math. Models Methods Appl. Sci., **4**, 571–587 (1994)

[5] Ciarlet, Ph.: The Finite Element Method for Elliptic Problems. North-Holland Publishing Company, Amsterdam (1978)

[6] Clément, Ph.: Approximation by finite element functions using local regularization. RAIRO Anal. Numér., **2**, 77–84 (1975)

[7] Courty, F., Leservoisier, D., George, P.L., Dervieux, A.: Continuous metrics and mesh optimization. Submitted for publication in Appl. Numer. Math. (2003)

[8] Darmofal, D.L., Venditti, D.A.: Anisotropic grid adaptation for functional outputs: application to two-dimensional viscous flows. J. Comput. Phys., **187**, 22–46 (2003)

[9] Eriksson, K., Johnson, C.: Adaptive streamline diffusion finite element methods for stationary convection-diffusion problems. Math. Comput., **60**, 167–188 (1993)

[10] Formaggia, L., Perotto, S.: New anisotropic a priori error estimates. Numer. Math., **89**, 641–667 (2001)

[11] Formaggia, L., Perotto, S., Zunino, P.: An anisotropic a-posteriori error estimate for a convection-diffusion problem. Comput. Visual. Sci., **4**, 99–104 (2001)

[12] Formaggia, L., Perotto, S.: Anisotropic error estimates for elliptic problems. Numer. Math., **94**, 67–92 (2003)

[13] Formaggia, L., Micheletti, S., Perotto, S.: Anisotropic mesh adaptation in Computational Fluid Dynamics: application to the advection-diffusion-reaction and the Stokes problems. Submitted for publication in Mathematics and Computers in Simulation (2003)

[14] Hecht, F.: BAMG: bidimensional anisotropic mesh generator. http://www-rocq.inria.fr/gamma/cdrom/www/bamg/eng.htm (1998)

[15] Kunert, G.: A Posteriori Error Estimation for Anisotropic Tetrahedral and Triangular Finite Element Meshes. Ph.D. thesis, Fakultät für Mathematik der Technischen Universität Chemnitz, Chemnitz (1999)

[16] Lions, J.L., Magenes, E.: Non-Homogeneous Boundary Value Problems and Applications. Volume I, Springer-Verlag, Berlin (1972)

[17] Micheletti, S., Perotto, S., Picasso, M.: Stabilized finite elements on anisotropic meshes: a priori error estimates for the advection-diffusion and Stokes problems. SIAM J. Numer. Anal., **41** No. 3, 1131–1162 (2003)

[18] Picasso, M.: An anisotropic error indicator based on Zienkiewicz-Zhu error estimator: application to elliptic and parabolic problems. SIAM J. Sci. Comput., **24** No. 4, 1328–1355 (2003)

[19] Siebert, K.G.: An a posteriori error estimator for anisotropic refinement. Numer. Math., **73**, 373–398 (1996)